

Axion oscillations in binary systems: angle-action surgery

VINCENT DESJACQUES,^{1,2} EVGENI GRISHIN,¹ AND YONADAV BARRY GINAT¹¹*Physics department, Technion – Israel Institute of Technology, Haifa 3200003, Israel*²*Asher Space Science Institute, Technion, Haifa 3200003, Israel*

ABSTRACT

Scalar, tensor waves induce oscillatory perturbations in Keplerian systems which can be probed with measurements of pulsar timing residuals. In this paper, we consider the imprint of coherent oscillations produced by ultra-light axion dark matter on the Roemer time delay. We use the angle-action formalism to calculate the time evolution of the observed signal and its dependence on the orbital parameters and the axion phase. We emphasize the similarity of the expected signal-to-noise with the response of an harmonic oscillator to an external oscillatory driving. We validate our theoretical predictions with numerical simulations. Our results furnish a useful benchmark for numerical codes and analysis procedures and, hopefully, will motivate the search for such imprints in real data.

Keywords: binaries: general, celestial mechanics, cosmology: theory, dark matter

1. INTRODUCTION

Gravitational radiation can resonate with binary systems and produce orbital perturbations potentially detectable (Rudenko 1975; Mashhoon 1978; Turner 1979). When the perturbations arise from a stochastic background of gravitational waves, monitoring the randomness of the orbital elements - through the correlation functions of frequency shifts and timing residuals of pulsars for instance - can set constraints on the amplitude of such a background (Mashhoon et al. 1981; Mashhoon 1985; Hui et al. 2013). This effect also takes place when a binary system is excited by scalar waves (Annunziatella et al. 2018), or embedded in a coherent background of very light bosons (Khmelnitsky & Rubakov 2014; Blas et al. 2017; Bokovi et al. 2018).

At low redshift, light bosons such as ultra-light axions form a Bose-Einstein condensate which oscillates coherently (unlike a stochastic background) on a timescale $\propto m_a^{-1}$ inversely proportional to the mass m_a of the axion particle (see, e.g., Marsh 2016; Hui et al. 2017; Niemeyer 2019, and references therein). Constraints on m_a have been set using Lyman- α forest measurements (Iršič et al. 2017; Armengaud et al. 2017; Kobayashi et al. 2017) and CMB lensing (Hložek et al. 2018) on Megaparsec scales; dwarf spheroidal (Marsh & Pop

2015; González-Morales et al. 2017; Safarzadeh & Spergel 2019; Broadhurst et al. 2019) and ultra-diffuse galaxies (Wasserman et al. 2019) on Kiloparsec scales; galactic core observations on (sub)parsec scales (Desjacques & Nusser 2019; Bar et al. 2019; Davies & Mocz 2020). Pulsar timing offers another avenue to probe the existence of coherent oscillations induced by ultra-light scalar fields (Khmelnitsky & Rubakov 2014; Blas et al. 2017; De Martino et al. 2017). Upper limits on the amplitude of such an oscillating gravitational potential in the Milky-Way halo have already been derived from pulsar timing arrays (PTAs) (Porayko & Postnov 2014; Porayko et al. 2018). Cross-correlation of residuals from different pulsar should improve these constraints (Hellings & Downs 1983).

Axion coherent oscillations also resonate with binary pulsars (Blas et al. 2019). While the effect is strongest near resonance, the very small width of the latter (when the coupling is purely gravitational) implies that one shall monitor instantaneous variations (Rozner et al. 2019) or the secular drift of orbital elements (Blas et al. 2019) away from resonances.

Mashhoon (1978) used Lagrange's planetary equations to develop an approximate theory of the interaction of a weak gravitational wave with a Keplerian binary. In this paper, we use angle-action variables to investigate the instantaneous variations (that is, not averaged over one orbital time) of a Keplerian system produced by a oscillating background of axion dark matter. We refer

Corresponding author: Vincent Desjacques
dvince@physics.technion.ac.il

the reader to [Binney & Tremaine \(1987\)](#) for an overview of the angle-action formalism.

The paper is organized as follows. After a brief presentation of the astrophysical/cosmological context and our numerical implementation in Section §2, we solve for the time evolution of the perturbed binary system using angle-action variables in Section §3. We explore the instantaneous variations of the Roemer time delay as a function of orbital parameters etc. in Section §4. We conclude in §5.

2. SETUP

We will use the numerical simulations of [Rozner et al. \(2019\)](#) to validate our theoretical predictions. We consider a binary pulsar system with total mass $M = m_1 + m_2$ and reduced mass $\mu = m_1 m_2 / (m_1 + m_2)$. The motion of the binary pulsar is integrated along with the perturbation induced by the coherent axion oscillations using the publicly available framework `REBOUND` ([Rein & Liu 2012](#)) and the fast, adaptive, high-order integrator `IAS15` for gravitational dynamics ([Rein & Spiegel 2015](#)), accurate to machine precision over a billion orbits.

In all the subsequent illustrations, we adopt the same parameters as [Rozner et al. \(2019\)](#), that is,

- A dark matter density $\rho_{\text{DM}} = 5 \times 10^3 \text{ M}_\odot \text{pc}^{-3}$
- An axion mass $m_a = 10^{-30} \text{ GeV}$
- An axion phase $\alpha = 0$
- A total binary mass $M = 2 \text{ M}_\odot$

The value of ρ_{DM} is comparable to the density ρ_c achieved near the hypothetical axion core (of radius $R_c \sim 1 \text{ pc}$) located in the vicinity of the Milky-Way halo center when the axion mass is 10^{-30} GeV ([Chavhanis 2011](#)). In the solar neighborhood, the dark matter density is smaller by four orders of magnitude, $\rho_{\text{DM}} \sim 0.3 \text{ M}_\odot \text{pc}^{-3}$. Furthermore, we conveniently define

$$\omega_a \equiv 2m_a. \quad (1)$$

At the fundamental resonance for which $\Omega = \Omega_0 = \omega_a$, the orbital frequency is $\Omega_0 \simeq 3.062 \times 10^{-6}$, and the semi major axis is $a_0 \simeq 0.205 \text{ AU}$. Finally, note that the axion phase $\alpha \equiv \alpha(\mathbf{x})$ generally is a function of the spatial position \mathbf{x} and, thus, actually varies among binary pulsar systems.

Following [Rozner et al. \(2019\)](#), we will focus on the signal imprinted in the Roemer time delay, which can be extracted from measurements of the pulse times of arrival (TOAs) at the detector. The Roemer time delay is the variation of the light travel time due to perturbations in the distance between the detector and the pulsar. In plain words, axion coherent oscillations induce

a perturbation $\delta \mathbf{r}(t)$ to the separation vector of the binary system at a given time t . Ignoring the apparent viewing geometry of the latter for simplicity, this translates into a perturbation $\Delta t_{\text{TOA}}(t_i) = \frac{1}{c} |\delta \mathbf{r}(t_i)|$ (c is the speed of light) in the pulse TOAs. The signal-to-noise ratio (SNR) for this effect can be expressed as

$$\left(\frac{S}{N} \right)^2 = \frac{1}{\sigma_\Delta^2} \sum_{i=1}^N (\Delta t_{\text{TOA}})^2(t_i), \quad (2)$$

where $t_i = i * \Delta$ are the times at which a TOA measurement is performed and σ_Δ is the error on the TOA for a pulse shape averaged over a time interval Δ . In what follows, we shall adopt $\sigma_\Delta = 10^{-6} \text{ s}$ for $\Delta = 10 \text{ s}$. The (ideal) number of measurements is $N = t_{\text{obs}} / \Delta$, where t_{obs} is the total time of observations. In practice, TOA measurements will be performed only a fraction f_{obs} of the time. We shall hereafter assume $f_{\text{obs}} = 10^{-3}$.

Eq.(2) is the sole observable we shall consider here as the Roemer delay is the largest effect in magnitude. However, the results presented in Sec. §3.4 can be used to calculate the signals imprinted in other delays (see e.g. [Edwards et al. 2006](#), for a detailed overview of timing models).

3. THE AXION PERTURBATION IN ANGLE-ACTION FORMALISM

To illustrate the power of the angle-action formalism, we will use the Delaunay variables. For simplicity however, we will focus on the 2-dimensional dynamics (justified since the angular momentum vector is conserved also in the perturbed system). Therefore, we can restrict ourselves to the Delaunay angles $\theta_\alpha = \{\theta_b, \theta_c\}$ and actions $J_\alpha = \{J_b, J_c\}$ (they correspond to the angles $\{\theta_2, \theta_3\}$ and actions $\{J_2, J_3\}$ in [Binney & Tremaine \(1987\)](#)). We will designate the polar variables as $q_\alpha = \{r, \vartheta\}$ and $p_\alpha = \{p_r, p_\vartheta\}$.

3.1. Hamiltonian

The total Hamiltonian of the system is $\mathcal{H} = \mathcal{H}_0 + \mathcal{H}_1$. The unperturbed Hamiltonian

$$\mathcal{H}_0(J_c) = -\frac{\mu k^2}{2J_c^2}, \quad (3)$$

where $k = GM\mu$, describes the Keplerian motion. In polar coordinates, the perturbation Hamiltonian takes the form

$$\begin{aligned} \mathcal{H}_1 &= 2\pi G \rho_{\text{DM}} \mu \cos(\omega_a t + \alpha) r^2 \\ &\equiv \mu \epsilon \Omega^2 a^2 \cos(\omega_a t + \alpha) \left(\frac{r}{a} \right)^2. \end{aligned} \quad (4)$$

Here, a and Ω are the semi-major axis and frequency of the binary. The amplitude of the perturbation Hamiltonian relative to \mathcal{H}_0 is quantified by the small parameter

$$\epsilon = \frac{2\pi\rho_{\text{DMA}}a^3}{M} = \epsilon_0 \left(\frac{a}{a_0} \right)^3, \quad (5)$$

where ϵ_0 is evaluated at the fundamental resonance. For our fiducial parameters (see Sec. §2), it is

$$\epsilon_0 = \frac{2\pi\rho_{\text{DMA}}a_0^3}{M} \simeq 3.073 \times 10^{-14}. \quad (6)$$

This justifies a perturbative treatment at first order in ϵ . The a^3 -scaling reflects the fact that $|\mathcal{H}_0| \sim \frac{1}{a}$, while

$$|\mathcal{H}_1| \sim \epsilon\Omega^2a^2 \sim \epsilon_0 \left(\frac{a}{a_0} \right)^3 a^{-3}a^2 \sim a^2. \quad (7)$$

As expected, the effect of axion oscillations increase with the physical volume enclosed by the binary motion.

Using the definition of ϵ , together with Kepler's third law $\Omega^2a^3 = GM$ and the relation $a = J_c^2/\mu k$, the overall multiplicative factor in \mathcal{H}_1 can be conveniently expressed as

$$\frac{1}{2}\mu\epsilon\Omega^2a^2 = \frac{1}{2}\frac{\epsilon_0}{a_0^3}\frac{J_c^4}{\mu^2k}. \quad (8)$$

Furthermore, the Fourier cosine decomposition of $(r/a)^2$ on the unperturbed Keplerian orbit (justified by the smallness of ϵ), for which θ_c equals the mean anomaly \mathcal{M} , reads

$$\left(\frac{r}{a} \right)^2 = 1 + \frac{3}{2}e^2 - \sum_{n=1}^{\infty} \frac{4}{n^2} J_n(ne) \cos(n\theta_c), \quad (9)$$

Here and henceforth, $0 \leq e < 1$ will denote the eccentricity. As a result, the perturbation Hamiltonian in the angle-action variables can be recast into the form

$$\mathcal{H}_1(\theta_c, J_b, J_c; t) = \frac{1}{2} \frac{\epsilon_0}{a_0^3} \frac{J_c^4}{\mu^2k} \left\{ \cos(\omega_a t + \alpha) \left(5 - 3 \frac{J_b^2}{J_c^2} \right) - \sum_{n=1}^{\infty} \frac{4}{n^2} J_n(ne) \left[\cos(\omega_a t + n\theta_c + \alpha) + \cos(\omega_a t - n\theta_c + \alpha) \right] \right\} \quad (10)$$

where it is understood that $e \equiv \sqrt{1 - J_b^2/J_c^2}$. Note also that $\frac{\epsilon_0}{a_0^3} \frac{J_c^3}{\mu^2k} = \epsilon\Omega$.

Eq.(10) will be useful for the computation of the time evolution of the perturbations (presented in Sec. §3.4).

3.2. Perturbed displacement

In the variables $(\theta_b, \theta_c, J_b, J_c)$, the separation vector $\mathbf{r}(t)$ takes the general form

$$\mathbf{r}(t) = \mathbf{r}(\theta_b(t), \theta_c(t), J_b(t), J_c(t)). \quad (11)$$

The time dependence of the angle - action variables is governed by Hamilton equations:

$$\dot{\theta}_\alpha = +\frac{\partial \mathcal{H}}{\partial J_\alpha}, \quad \dot{J}_\alpha = -\frac{\partial \mathcal{H}}{\partial \theta_\alpha}, \quad (12)$$

$$\mathcal{H} = \mathcal{H}_0(J_c) + \mathcal{H}_1(\theta_c, J_b, J_c; t).$$

The unperturbed solution given by \mathcal{H}_0 is

$$\mathbf{r}_0(t) = \mathbf{r}(\theta_b^0(t), \theta_c^0(t), J_b^0(t), J_c^0(t)) \quad (13)$$

with

$$\theta_b^0(t) = 0, \quad \theta_c^0(t) = \mathcal{M}(t), \quad (14)$$

$$J_b^0 = J_c^0 \sqrt{1 - e^2}, \quad J_c^0 = \sqrt{k\mu a}.$$

It will be convenient to parametrize the unperturbed orbit in terms of the eccentric anomaly ξ , and express the mean anomaly \mathcal{M} as $\mathcal{M}(\xi) = \xi - e \sin \xi$.

Combining the previous expressions, the displacement vector reads

$$\begin{aligned} \delta\mathbf{r}(t) &\equiv \mathbf{r}(t) - \mathbf{r}_0(t) \\ &\approx (\cos \vartheta, \sin \vartheta) \delta r + r(-\sin \vartheta, \cos \vartheta) \delta \vartheta \end{aligned} \quad (15)$$

at first order in the small perturbation $\epsilon \ll 1$, with

$$\begin{aligned} \delta r &= \frac{\partial r}{\partial \theta_\alpha} \bigg|_0 \Delta \theta_\alpha + \frac{\partial r}{\partial J_\alpha} \bigg|_0 \Delta J_\alpha \\ \delta \vartheta &= \frac{\partial \vartheta}{\partial \theta_\alpha} \bigg|_0 \Delta \theta_\alpha + \frac{\partial \vartheta}{\partial J_\alpha} \bigg|_0 \Delta J_\alpha. \end{aligned} \quad (16)$$

These relations follow from writing the position vector in polar coordinates, $\mathbf{r} = r(\cos \vartheta, \sin \vartheta)$. Since the perturbations $\Delta \theta_\alpha(t)$ and $\Delta J_\alpha(t)$ are first order in ϵ , the partial derivatives of the polar coordinates are computed on the unperturbed orbit. Furthermore, Einstein summation's convention is implied here and throughout this paper.

3.3. Generating function

To calculate the derivatives of the polar coordinates w.r.t. the angle-action variables. consider the function \mathcal{W} generating the canonical transformation to the De-

launay variables,

$$\mathcal{W}(r, \vartheta, J_b, J_c) \equiv \int dr \operatorname{sgn}(\dot{r}) \sqrt{-\frac{\mu^2 k^2}{J_c^2} + \frac{2\mu k}{r} - \frac{J_b^2}{r^2}} + J_b \vartheta, \quad (17)$$

and notice that the first of the two equations of canonical transformations

$$\theta_b = \frac{\partial \mathcal{W}}{\partial J_b} \quad \text{and} \quad \theta_c = \frac{\partial \mathcal{W}}{\partial J_c} \quad (18)$$

involves the variables $(r, \vartheta, \theta_b, J_b, J_c)$, while the second involves only (r, θ_c, J_b, J_c) . Therefore, we can write Eq.(18) as $g_1 = g_2 = 0$. The auxiliary functions g_1 and g_2 are

$$\begin{aligned} g_1(r, \vartheta, \theta_b, J_b, J_c) &\equiv \theta_b - \frac{\partial \mathcal{W}}{\partial J_b}, \\ g_2(r, \theta_c, J_b, J_c) &\equiv \theta_c - \frac{\partial \mathcal{W}}{\partial J_c}, \end{aligned} \quad (19)$$

with the understanding that all the variables should be treated as independent. Next, we can solve $g_2 = 0$ for $r = r(\theta_c, J_b, J_c)$, which we subsequently substitute into $g_1 = 0$ to solve for $\vartheta = \vartheta(\theta_b, \theta_c, J_b, J_c)$.

In differential form, we have

$$\begin{aligned} dg_1 &= \frac{\partial g_1}{\partial r} dr + \frac{\partial g_1}{\partial \vartheta} d\vartheta + \frac{\partial g_1}{\partial \theta_b} d\theta_b + \frac{\partial g_1}{\partial J_b} dJ_b + \frac{\partial g_1}{\partial J_c} dJ_c \\ dg_2 &= \frac{\partial g_2}{\partial r} dr + \frac{\partial g_2}{\partial \theta_c} d\theta_c + \frac{\partial g_2}{\partial J_b} dJ_b + \frac{\partial g_2}{\partial J_c} dJ_c. \end{aligned} \quad (20)$$

Setting $dg_2 = 0$ implies

$$dr = -\left(\frac{\partial g_2}{\partial r}\right)^{-1} \left(\frac{\partial g_2}{\partial \theta_c} d\theta_c + \frac{\partial g_2}{\partial J_b} dJ_b + \frac{\partial g_2}{\partial J_c} dJ_c \right) \quad (21)$$

Now, since Eq.(18) implies $\frac{\partial g_2}{\partial \theta_c} = 1$, we find

$$\begin{aligned} \frac{\partial r}{\partial \theta_c} &= -\left(\frac{\partial g_2}{\partial r}\right)^{-1} \frac{\partial g_2}{\partial \theta_c} \\ &= -\left(\frac{\partial g_2}{\partial r}\right)^{-1} \\ &= +\left[\frac{\partial}{\partial r} \left(\frac{\partial \mathcal{W}}{\partial J_c}\right)\right]^{-1}. \end{aligned} \quad (22)$$

Similarly,

$$\begin{aligned} \frac{\partial r}{\partial J_b} &= -\left(\frac{\partial g_2}{\partial r}\right)^{-1} \frac{\partial g_2}{\partial J_b} = -\frac{\partial r}{\partial \theta_c} \frac{\partial}{\partial J_b} \left(\frac{\partial \mathcal{W}}{\partial J_c}\right) \\ \frac{\partial r}{\partial J_c} &= -\left(\frac{\partial g_2}{\partial r}\right)^{-1} \frac{\partial g_2}{\partial J_c} = -\frac{\partial r}{\partial \theta_c} \frac{\partial}{\partial J_c} \left(\frac{\partial \mathcal{W}}{\partial J_c}\right). \end{aligned} \quad (23)$$

To proceed further, we need

$$\frac{\partial \mathcal{W}}{\partial J_b} = \vartheta - \operatorname{sgn}(\dot{r}) \arccos \left(\frac{\frac{J_b^2}{\mu k r} - 1}{\sqrt{1 - \frac{J_b^2}{J_c^2}}} \right) \quad (24)$$

$$\begin{aligned} \frac{\partial \mathcal{W}}{\partial J_c} &= \operatorname{sgn}(\dot{r}) \left[-\frac{r}{J_c} \sqrt{-\frac{\mu^2 k^2}{J_c^2} + \frac{2\mu k}{r} - \frac{J_b^2}{r^2}} \right. \\ &\quad \left. + \arccos \left(\frac{1 - \frac{\mu k r}{J_c^2}}{\sqrt{1 - \frac{J_b^2}{J_c^2}}} \right) \right]. \end{aligned}$$

In the second equality, the first term in the right-hand side vanishes at the pericenter and apocenter, i.e. $r = r_{\pm} = 1 \pm e$. Note also that $\arccos(x)$ is defined on its main branch $-\pi \leq x < \pi$. Therefore, these derivatives must be properly incremented (that is, subtract and add $\operatorname{Int}(\xi/2\pi + 1/2)$ to the first and second line, respectively) such that the angles θ_b and θ_c grow monotonically with time.

Parametrizing the unperturbed trajectory with the eccentric anomaly ξ , the radial coordinate reads $r(\xi) = a(1 - e \cos \xi)$ and the partial derivatives of r reduce to

$$\begin{aligned} \left. \frac{\partial r}{\partial \theta_b} \right|_0 &= 0 \\ \left. \frac{\partial r}{\partial \theta_c} \right|_0 &= \frac{ae \sin \xi}{(1 - e \cos \xi)} \\ \left. \frac{\partial r}{\partial J_b} \right|_0 &= \frac{a}{J_c} \frac{\sqrt{1 - e^2}}{e} \frac{(e - \cos \xi)}{(e \cos \xi - 1)} \\ \left. \frac{\partial r}{\partial J_c} \right|_0 &= \frac{a}{J_c} \frac{(-3e + \cos \xi + 3e^2 \cos \xi - e^3 \cos(2\xi))}{e(e \cos \xi - 1)}. \end{aligned} \quad (25)$$

In this derivation, it is essential to take into account the multiplicative factor of $\operatorname{sgn}(\dot{r}) = \operatorname{sgn}(\sin \xi)$ in the generating function $\mathcal{W}(r, \vartheta, J_b, J_c)$ as it ensures that all the partial derivatives are continuous functions of ξ .

The calculation of the derivatives $\partial \vartheta / \partial \theta_\alpha$ and $\partial \vartheta / \partial J_\alpha$ proceeds analogously. Setting $dg_1 = 0$, substituting $r = r(\theta_c, J_b, J_c)$ and taking advantage of the fact that $\frac{\partial g_1}{\partial \vartheta} = -\frac{\partial}{\partial \vartheta} \frac{\partial \mathcal{W}}{\partial J_b} = -1$, we obtain

$$\begin{aligned} d\vartheta &= \left[\frac{\partial g_1}{\partial \theta_b} d\theta_b + \frac{\partial g_1}{\partial r} \frac{\partial r}{\partial \theta_c} d\theta_c + \left(\frac{\partial g_1}{\partial J_b} + \frac{\partial g_1}{\partial r} \frac{\partial r}{\partial J_b} \right) dJ_b \right. \\ &\quad \left. + \left(\frac{\partial g_1}{\partial J_c} + \frac{\partial g_1}{\partial r} \frac{\partial r}{\partial J_c} \right) dJ_c \right]. \end{aligned} \quad (26)$$

For instance, we read off

$$\begin{aligned} \frac{\partial \vartheta}{\partial J_b} &= \frac{\partial g_1}{\partial J_b} + \frac{\partial g_1}{\partial r} \frac{\partial r}{\partial J_b} \\ &= -\frac{\partial}{\partial J_b} \left(\frac{\partial \mathcal{W}}{\partial J_b} \right) - \frac{\partial r}{\partial J_b} \frac{\partial}{\partial r} \left(\frac{\partial \mathcal{W}}{\partial J_b} \right). \end{aligned} \quad (27)$$

After some algebra, we arrive at

$$\begin{aligned} \left. \frac{\partial \vartheta}{\partial \theta_b} \right|_0 &= 1 \\ \left. \frac{\partial \vartheta}{\partial \theta_c} \right|_0 &= \frac{\sqrt{1 - e^2}}{(1 - e \cos \xi)^2} \end{aligned} \quad (28)$$

$$\begin{aligned}\frac{\partial \vartheta}{\partial J_b} \Big|_0 &= \frac{1}{J_c} \frac{(-2 + e^2 + e \cos \xi)}{e(1 - e \cos \xi)^2} \sin \xi \\ \frac{\partial \vartheta}{\partial J_c} \Big|_0 &= \frac{1}{J_c} \frac{\sqrt{1 - e^2}}{e} \frac{(2 - e^2 - e \cos \xi)}{(1 - e \cos \xi)^2} \sin \xi.\end{aligned}$$

One can check that the following (equal time) Poisson bracket vanishes identically for any ξ ,

$$[r, \vartheta]_{\theta_\alpha, J_\alpha} \equiv 0. \quad (29)$$

This indicates that the various partial derivatives we computed are consistent with a canonical transformation, as it should be. Note that $[r, \vartheta]$ does not generally vanish when r and ϑ are evaluated at different times on the physical trajectory.

To conclude this Section, one could in principle transform to a new set of angle-action coordinates constructed such that the perturbed Hamiltonian depends on the new action variables solely (up to first order in ϵ). This standard procedure is briefly reviewed in, e.g.,

[Annulli et al. \(2018\)](#). However, it does not give any practical advantage in the computation of the signal we are aiming at. Therefore, we have not implemented it here.

3.4. Time evolution

Next, we compute the perturbations $\Delta\theta_\alpha(t)$ and $\Delta J_\alpha(t)$ to the angle-action variables from the perturbation Hamiltonian Eq.(4). We require that the perturbed and unperturbed orbit coincide initially (that is, at the beginning of the observational period), so that $\Delta\theta_\alpha$ and ΔJ_α vanish at $t = 0$. We will denote the initial eccentric and mean anomaly as ξ_0 and \mathcal{M}_0 , respectively. On the unperturbed trajectory, we thus have $\theta_c^0(t) = \mathcal{M}(t) = \Omega t + \mathcal{M}_0$, with $\mathcal{M}_0 = \xi_0 - e \sin \xi_0$. The offset between the periaxis passages and the peaks of the axion oscillatory forcing evolves with time depending on the initial conditions (α, \mathcal{M}_0) and the frequencies (ω_a, Ω) unless one sits at a resonance (in which case only α and \mathcal{M}_0 matter).

For the angles, Hamilton equations give

$$\begin{aligned}\Delta\theta_b(t) &= \int_0^t dt' \frac{\partial \mathcal{H}_1}{\partial J_b} \\ &= -3\epsilon \left(\frac{\Omega}{\omega_a} \right) \sqrt{1 - e^2} \left(\sin(\omega_a t + \alpha) - \sin \alpha \right) + 2\epsilon \left(\frac{\Omega}{\omega_a} \right) \frac{\sqrt{1 - e^2}}{e} \sum_{n=1}^{\infty} \frac{J'_n(ne)}{n} \mathcal{S}_{n1}^{(+)}(\omega_a, \Omega, \alpha, \mathcal{M}_0; t)\end{aligned} \quad (30)$$

$$\begin{aligned}\Delta\theta_c(t) &= \int_0^t dt' \left(-3 \frac{\Omega}{J_c} \Delta J_c + \frac{\partial \mathcal{H}_1}{\partial J_c} \right) \\ &= -6\epsilon \left(\frac{\Omega}{\omega_a} \right) \sum_{n=1}^{\infty} \frac{J_n(ne)}{n} \left[\left(\frac{\Omega}{\omega_a} \right) \mathcal{S}_{n2}^{(-)}(\omega_a, \Omega, \alpha, \mathcal{M}_0; t) - \Omega t \mathcal{A}_n \left(\frac{\Omega}{\omega_a}, \alpha, \mathcal{M}_0 \right) \right] + \epsilon \left(\frac{\Omega}{\omega_a} \right) (7 + 3e^2) \\ &\quad \times \left(\sin(\omega_a t + \alpha) - \sin \alpha \right) - 2\epsilon \left(\frac{\Omega}{\omega_a} \right) \sum_{n=1}^{\infty} \left[4 \frac{J_n(ne)}{n^2} + \left(\frac{1 - e^2}{e} \right) \frac{J'_n(ne)}{n} \right] \mathcal{S}_{n1}^{(+)}(\omega_a, \Omega, \alpha, \mathcal{M}_0; t)\end{aligned} \quad (31)$$

whereas, for the actions, we have

$$\Delta J_b(t) = - \int_0^t dt' \frac{\partial \mathcal{H}_1}{\partial \theta_b} = 0, \quad (32)$$

which expresses the conservation of angular momentum, and

$$\Delta J_c(t) = - \int_0^t dt' \frac{\partial \mathcal{H}_1}{\partial \theta_c} = 2\epsilon \left(\frac{\Omega}{\omega_a} \right) J_c \sum_{n=1}^{\infty} \frac{J_n(ne)}{n} \mathcal{C}_{n1}^{(-)}(\omega_a, \Omega, \alpha, \mathcal{M}_0; t). \quad (33)$$

To derive all these expressions, we have substituted the unperturbed solution $\theta_c = \theta_c^0(t)$, and taken advantage of the relations $J_c = \mu \Omega a^2$ and $\Omega = \mu k^2 / J_c^3$ to simplify them further.

For shorthand convenience, we have also introduced the functions $\mathcal{S}_{nq}^{(\pm)}(\omega_a, \Omega, \alpha, \mathcal{M}_0; t)$ and $\mathcal{C}_{nq}^{(\pm)}(\omega_a, \Omega, \alpha, \mathcal{M}_0; t)$ defined as

$$\mathcal{S}_{nq}^{(\pm)} = \frac{\sin(\omega_a t + n\Omega t + \alpha + n\mathcal{M}_0) - \sin(\alpha + n\mathcal{M}_0)}{\left(1 + n \frac{\Omega}{\omega_a}\right)^q} \pm \frac{\sin(\omega_a t - n\Omega t + \alpha - n\mathcal{M}_0) - \sin(\alpha - n\mathcal{M}_0)}{\left(1 - n \frac{\Omega}{\omega_a}\right)^q}, \quad (34)$$

$$\mathcal{C}_{nq}^{(\pm)} = \frac{\cos(\omega_a t + n\Omega t + \alpha + n\mathcal{M}_0) - \cos(\alpha + n\mathcal{M}_0)}{\left(1 + n\frac{\Omega}{\omega_a}\right)^q} \pm \frac{\cos(\omega_a t - n\Omega t + \alpha - n\mathcal{M}_0) - \cos(\alpha - n\mathcal{M}_0)}{\left(1 - n\frac{\Omega}{\omega_a}\right)^q}.$$

The (\pm) determines their parity under the transformation $n \rightarrow -n$. Furthermore, both $\mathcal{S}_{nq}^{(\pm)}$ and $\mathcal{C}_{nq}^{(\pm)}$ vanish at the initial time $t = 0$.

For $\Delta\theta_c$, the expression is somewhat more involved because one needs to consider two variations:

$$\Delta\dot{\theta}_c = \Delta \left(\frac{\partial \mathcal{H}_0}{\partial J_c} \right) + \frac{\partial \mathcal{H}_1}{\partial J_c} = \frac{\partial \Omega}{\partial J_c} \Delta J_c + \frac{\partial \mathcal{H}_1}{\partial J_c}. \quad (35)$$

The first term in the right-hand side is the perturbation to the Keplerian frequency. As a result, the angle θ_c

$$-3 \frac{\Omega}{J_c} \int_0^t dt' \Delta J_c(t') = -6\epsilon \left(\frac{\Omega}{\omega_a} \right) \sum_{n=1}^{\infty} \frac{J_n(ne)}{n} \left[\left(\frac{\Omega}{\omega_a} \right) \mathcal{S}_{n2}^{(-)}(\omega_a, \Omega, \mathcal{M}_0, \alpha; t) - \Omega t \mathcal{A}_n \left(\frac{\Omega}{\omega_a}, \alpha, \mathcal{M}_0, \right) \right], \quad (36)$$

in which the time-independent function $\mathcal{A}_n(x, \alpha, \mathcal{M}_0)$ is

$$\mathcal{A}_n = \frac{\cos(\alpha - n\mathcal{M}_0)}{(1 - nx)} - \frac{\cos(\alpha + n\mathcal{M}_0)}{(1 + nx)}. \quad (37)$$

This is the first term in the right-hand side of Eq.(31). Observe that, in the limit $\frac{\Omega}{\omega_a} \rightarrow 0$, the square brackets scales like Ω^2 and, consequently, this effect becomes subdominant when $a \gg a_0$.

To validate our analytical results, we numerically evolved the perturbed and unperturbed system in polar coordinates and extracted the time evolution of δr and $\delta\vartheta$, which we compared to our theoretical prediction obtained upon combining Eqs. (30) – (33) with the partial derivatives Eq. (25) and Eq. (28). In practice, we truncated the series expansion of \mathcal{H}_1 at the 20th harmonic. The results are shown in Fig.1 as a function of the eccentric anomaly ξ . The initial conditions were set at pericenter passage ($\mathcal{M}_0 = \xi_0 = 0$). They assume a highly eccentric orbit with $e \approx 0.866$. As a consequence, the change in orbital frequency is the dominant effect. This translates into a fairly large perturbation in the polar angle $\delta\vartheta$ (relative to δr) owing to the term $\frac{\partial\vartheta}{\partial\theta_c} \Delta\theta_c$, which peaks at pericenter passage. Note that δr is shown in unit of the semi-major axis a .

We emphasize that our calculation is valid everywhere except in small neighborhoods of size $\sqrt{\epsilon}$ centered on the resonances. The near resonance case is thoroughly discussed in Blas et al. (2017); Rozner et al. (2019). Note also that the angle perturbations Eq.(30) - (31)

evolves faster (or slower) relative to the unperturbed case. We have

$$\frac{\partial \Omega}{\partial J_c} \Delta J_c = -3 \frac{\Omega}{J_c} \Delta J_c.$$

This effect vanishes at first order for a perfectly circular orbit ($e = 0$) because the unperturbed orbit sits at the bottom of the effective 1-body (radial) potential. As a consequence, any variation in the frequency - or energy - must be second order for the circular case. Using Eq.(33) and integrating over time, this becomes

do not depend on the reduced mass μ of the system, while Eq.(33) does through the multiplicative factor of J_c . However, the latter cancels out in δr and $\delta\vartheta$. Hence, the perturbation δr to the separation vector truly are independent of the reduced mass, as requested by the Equivalence Principle.

4. SIGNAL-TO-NOISE FOR THE ROEMER DELAY

Having solved the equations of motion to first order in ϵ , we will now concentrate on the variations in Roemer time delay and the corresponding signal-to-noise as quantified in Sec. §2.

4.1. General expression

Taking into account a duty cycle of f_{obs} as advocated above, the SNR Eq.(2) for the perturbation to the Roemer time delay can be expressed as

$$\begin{aligned} \left(\frac{S}{N} \right)^2 &= \frac{f_{\text{obs}}}{\sigma_{\Delta}^2 \Delta} \sum_{i=1}^N \Delta \cdot (\Delta t_{\text{TOA}})^2(t_i) \\ &= \frac{f_{\text{obs}}}{\sigma_{\Delta}^2 \Delta} \int_0^{t_{\text{obs}}} dt \frac{|\delta r|^2}{c^2} \\ &= \epsilon^2 a^2 \left(\frac{\Omega}{\omega_a} \right)^2 \left(\frac{f_{\text{obs}} t_{\text{obs}}}{\sigma_{\Delta}^2 c^2 \Delta} \right) \left\{ \frac{1}{t_{\text{obs}}} \int_0^{t_{\text{obs}}} dt |\delta \tilde{r}|^2(t) \right\} \end{aligned} \quad (38)$$

where, for convenience, we have introduced a dimensionless displacement $\delta \tilde{r}(t)$ defined through the relation

$$\delta r(t) \equiv \epsilon a \left(\frac{\Omega}{\omega_a} \right) \delta \tilde{r}(t). \quad (39)$$

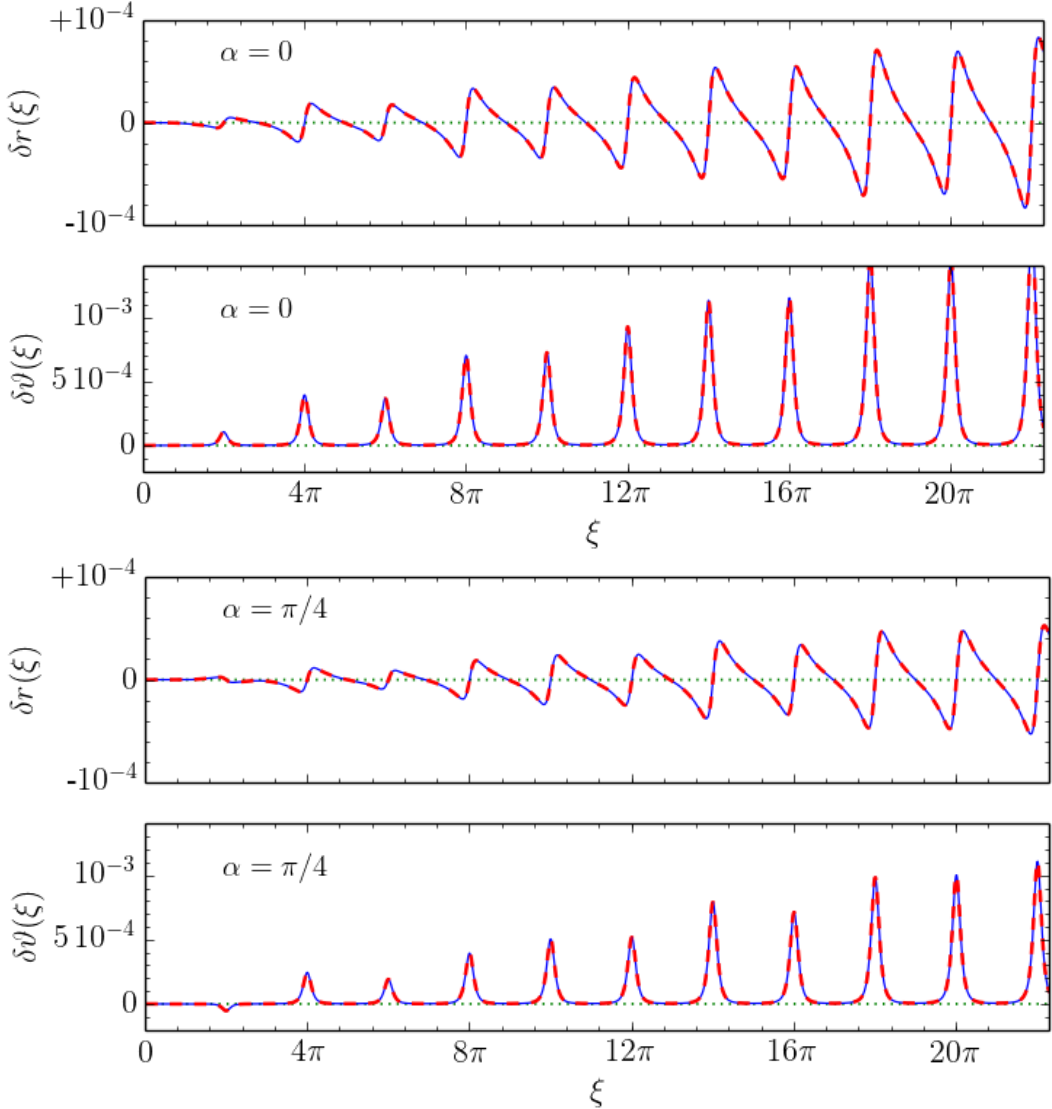


Figure 1. Time evolution of the coordinate perturbations $\delta r(\xi)$ and $\delta\vartheta(\xi)$ as a function of the eccentric anomaly ξ (see text for details). The solid (blue) curve is the results of a direct numerical integration in polar coordinates, while the dashed (red) curve show the theoretical prediction (at first order in ϵ). The phase is $\alpha = 0$ (top panels) and $\alpha = \pi/4$ (bottom panels). The other, common parameter values are $\epsilon_0 = 10^{-7}$, $\frac{\Omega}{\omega_a} \approx 1.713$, and $e \approx 0.866$. Note that δr is plotted in unit of the semi-major axis a .

The last two equalities in Eq.(38) assume that the sum over discrete times can be traded for an integral, which is a good approximation when the number of measurements is large.

To calculate the SNR, an expression for $|\delta\mathbf{r}|^2 = \delta r^2 + r^2\delta\vartheta^2$, with δr and $\delta\vartheta$ are given by Eq. (16), is required. For this purpose, it is convenient to use the eccentric anomaly ξ as a time variable, and recast Eq.(38) into

$$\left(\frac{S}{N}\right)^2 = \left(\frac{\epsilon\Omega a}{\omega_a}\right)^2 \left(\frac{f_{\text{obs}} t_{\text{obs}}}{\sigma_{\Delta}^2 c^2 \Delta}\right) \times \left\{ \frac{1}{\Omega t_{\text{obs}}} \int_{\xi_0}^{\xi_{\text{obs}} + \xi_0} d\xi (1 - e \cos \xi) |\delta\mathbf{r}|^2(\xi) \right\}, \quad (40)$$

where ξ_{obs} denotes the amount of eccentric anomaly elapsed during the observational run. The upper limit $\xi_{\text{obs}} = \xi_{\text{obs}}(t_{\text{obs}})$ of the integral is determined from $\Omega t_{\text{obs}} = \mathcal{M}(\xi_{\text{obs}}) - \mathcal{M}(\xi_0)$.

To get insight into the dependence of the SNR on the axion mass and the orbital parameters, consider the limit $\Omega \gg \omega_a$. In this regime, the perturbation produced by the axion coherent oscillations can be treated as time-independent. Therefore, Eq.(4) shows that they yield a force of amplitude $\epsilon\Omega r \sim \epsilon\Omega a$ per unit mass. This implies that the variation $\delta\dot{a}$ is

$$\delta\dot{a} = \int_0^T dt \delta\ddot{r} \sim \epsilon\Omega^2 a \int_0^T dt \sim \epsilon\Omega a \quad (41)$$

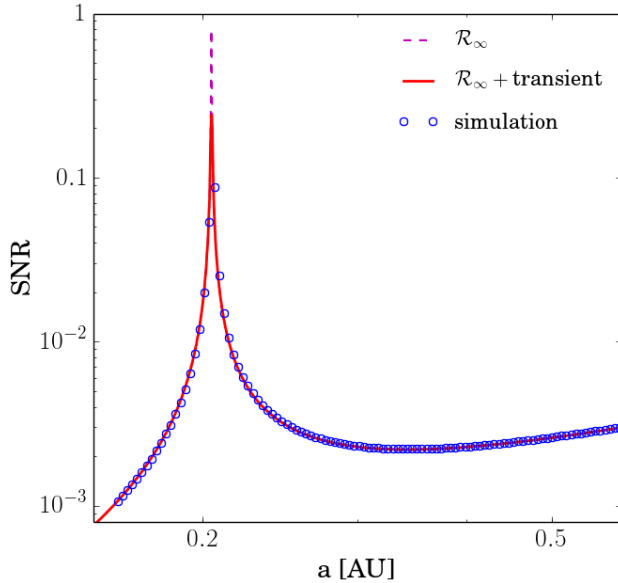


Figure 2. Signal-to-noise for a detection of the Roemer time delay in the case of a circular orbit ($e = 0$). The blue data points are the simulations, the solid (red) curve represents the long-time asymptotics prediction, Eq.(53), while the dashed (magenta) curve shows the full result including the transient contribution Eq.(52). For this run, we have artificially increased ϵ_0 by a factor of 10^5 in the simulations in order to mitigate the numerical noise. We have rescaled the final results so that they correspond to the fiducial model outlined in Sec. §2.

since the orbital period is $T = 2\pi/\Omega$. For a total observational time t_{obs} , the change δa thus is

$$\delta a \sim \int_0^{t_{\text{obs}}} dt \delta \dot{a} \sim \epsilon \Omega a t_{\text{obs}} \sim a^{5/2} t_{\text{obs}}. \quad (42)$$

Since the overall amplitude of the signal-to-noise ratio is proportional to

$$\epsilon \cdot \Omega \cdot a \propto a^3 \cdot a^{-3/2} \cdot a \propto a^{5/2}, \quad (43)$$

Eq.(42) suggests that the SNR should behave like $a^{5/2}$ in the limit $a \rightarrow 0$ or, equivalently, the curly brackets in Eq.(40) asymptotes to a constant in the same limit. We will see that this is indeed the case.

4.2. Development at small eccentricities

Emission of gravitational waves will eventually circularize the orbit of binary pulsar systems, so that $e \approx 0$ is

a very good approximation in the late stage of the coalescence phase (Peters 1964). Therefore, it is instructive to develop the previous results for low eccentricities. As we shall see now, the SNR can be cast into a simple expression in the limit $e \rightarrow 0$.

To proceed, we specialize the partial derivatives of the polar coordinates (r, ϑ) w.r.t. the angles and actions (along the unperturbed trajectory, which is now a circular orbit) to the case $e \rightarrow 0$:

$$\begin{aligned} \frac{\partial r}{\partial \theta_b} \Big|_0 &= 0 & (44) \\ \frac{\partial r}{\partial \theta_c} \Big|_0 &\approx ae \sin \xi + ae^2 \cos \xi \sin \xi \\ \frac{\partial r}{\partial J_b} \Big|_0 &\approx \frac{a}{e J_c} \cos \xi - \frac{a}{J_c} \sin^2 \xi + \frac{ae}{2 J_c} (\cos 2\xi - 2) \cos \xi \\ \frac{\partial r}{\partial J_c} \Big|_0 &\approx -\frac{a}{e J_c} \cos \xi + \frac{a}{2 J_c} (5 - \cos 2\xi) - \frac{ae}{J_c} \cos^3 \xi \\ \frac{\partial \vartheta}{\partial \theta_b} \Big|_0 &= 1 \\ \frac{\partial \vartheta}{\partial \theta_c} \Big|_0 &\approx 1 + 2e \cos \xi - \left(\frac{1}{2} - 3 \cos^2 \xi \right) e^2 \\ \frac{\partial \vartheta}{\partial J_b} \Big|_0 &\approx -\frac{2}{e J_c} \sin \xi - \frac{3}{J_c} \sin \xi \cos \xi - \frac{e}{J_c} (1 + 2 \cos 2\xi) \sin \xi \\ \frac{\partial \vartheta}{\partial J_c} \Big|_0 &\approx \frac{2}{e J_c} \sin \xi + \frac{3}{J_c} \sin \xi \cos \xi + \frac{e}{J_c} (\sin 3\xi - \sin \xi). \end{aligned}$$

In each expression, we retained terms up to order e except for the partial derivatives relative to θ_c , for which we include terms up to order e^2 (because the perturbation $\Delta \theta_c$ features a contribution of order e^{-1}). Although the derivatives relative to the actions diverge in the limit $e \rightarrow 0$, the relation $[r, \vartheta]_{\theta_\alpha, J_\alpha} = 0$ is always satisfied along the physical trajectory (i.e. when r and ϑ are evaluated at a fixed ξ).

We now turn to the expressions for $\Delta \theta_\alpha$ and ΔJ_α , and use the fact that, for small $ne \ll 1$, the Bessel functions behave like $J_n(ne) \sim (ne)^n$. In particular, $J_1(e) \approx e/2$. Writing $J'_n(ne) = J_{n-1}(ne) - \frac{1}{e} J_n(ne)$, Taylor-expanding the Bessel functions in the small argument limit and retaining terms up to order e (since the partial derivatives of r and ϑ w.r.t. the angles θ_b and θ_c are at best of order e^0), we find

$$\Delta \theta_b \xrightarrow{e \rightarrow 0} \epsilon \left(\frac{\Omega}{\omega_a} \right) \left\{ \frac{\mathcal{S}_{11}^{(+)}}{e} + \frac{\mathcal{S}_{21}^{(+)}}{2} - 3(\sin(\omega_a t + \alpha) - \sin \alpha) + \frac{1}{8} (-7\mathcal{S}_{11}^{(+)} + 3\mathcal{S}_{31}^{(+)})e + \mathcal{O}(e^2) \right\} \quad (45)$$

$$\Delta\theta_c \xrightarrow{e \rightarrow 0} -\epsilon \left(\frac{\Omega}{\omega_a} \right) \left\{ \frac{\mathcal{S}_{11}^{(+)}}{e} + \frac{\mathcal{S}_{21}^{(+)}}{2} - 7 \left(\sin(\omega_a t + \alpha) - \sin \alpha \right) + \left[\frac{3}{8} \left(7\mathcal{S}_{11}^{(+)} + \mathcal{S}_{31}^{(+)} \right) + 3 \left(\frac{\Omega}{\omega_a} \right) \mathcal{S}_{12}^{(-)} - 3\Omega t \mathcal{A}_1 \right] e + \mathcal{O}(e^2) \right\}.$$

All the functions $\mathcal{S}_{1q}^{(\pm)}$ and $\mathcal{C}_{1q}^{(\pm)}$ that appear in the previous expressions are evaluated at $t > 0$. Furthermore, although the individual deviations $\Delta\theta_b$ and $\Delta\theta_c$ diverge in the limit $e \rightarrow 0$, their contribution to the displacement $\delta\mathbf{r}$ is always well behaved since the latter depends on

$$\begin{aligned} \frac{\partial \vartheta}{\partial \theta_b} \Delta\theta_b + \frac{\partial \vartheta}{\partial \theta_c} \Delta\theta_c &= \epsilon \left(\frac{\Omega}{\omega_a} \right) \left\{ 4 \left(\sin(\omega_a t + \alpha) - \sin \alpha \right) - 2 \cos \xi \mathcal{S}_{11}^{(+)} + \left[- \left(3\mathcal{S}_{11}^{(+)} + 3 \cos^2 \xi \mathcal{S}_{11}^{(+)} + \cos \xi \mathcal{S}_{21}^{(+)} \right) \right. \right. \\ &\quad \left. \left. + 14 \left(\sin(\omega_a t + \alpha) - \sin \alpha \right) - 3 \left(\frac{\Omega}{\omega_a} \right) \mathcal{S}_{12}^{(-)} + 3\Omega t \mathcal{A}_1 \right] e + \mathcal{O}(e^2) \right\}. \end{aligned} \quad (46)$$

For the action variables, we have $\Delta J_b \equiv 0$ while

$$\Delta J_c \xrightarrow{e \rightarrow 0} \epsilon J_c \left(\frac{\Omega}{\omega_a} \right) \left[\mathcal{C}_{11}^{(-)} e + \frac{1}{2} \mathcal{C}_{21}^{(-)} e^2 + \mathcal{O}(e^3) \right]. \quad (47)$$

The term linear in e in ΔJ_c combines with that proportional to e^{-1} in $\frac{\partial \theta_c}{\partial J_c}$ to give a e^0 contribution. More precisely,

$$\frac{\partial \vartheta}{\partial J_b} \Delta J_b + \frac{\partial \vartheta}{\partial J_c} \Delta J_c = \epsilon \left(\frac{\Omega}{\omega_a} \right) \left[2 \sin \xi \mathcal{C}_{11}^{(-)} + \sin \xi \left(3 \cos \xi \mathcal{C}_{11}^{(-)} + \mathcal{C}_{21}^{(-)} \right) e + \mathcal{O}(e^2) \right]. \quad (48)$$

Applying the same analysis to the radial coordinate r eventually leads to

$$\begin{aligned} \frac{\partial r}{\partial \theta_b} \Delta\theta_b + \frac{\partial r}{\partial \theta_c} \Delta\theta_c &= -\epsilon a \left(\frac{\Omega}{\omega_a} \right) \left\{ \sin \xi \mathcal{S}_{11}^{(+)} + \sin \xi \left[\cos \xi \mathcal{S}_{11}^{(+)} + \frac{1}{2} \mathcal{S}_{21}^{(+)} - 3 \left(\sin(\omega_a t + \alpha) - \sin \alpha \right) \right] e + \mathcal{O}(e^2) \right\} \\ \frac{\partial r}{\partial J_b} \Delta J_b + \frac{\partial r}{\partial J_c} \Delta J_c &= -\epsilon a \left(\frac{\Omega}{\omega_a} \right) \left\{ \cos \xi \mathcal{C}_{11}^{(-)} + \left[\frac{1}{2} \left(\cos \xi \mathcal{C}_{21}^{(-)} + (\cos 2\xi - 3) \mathcal{C}_{11}^{(-)} \right) - \mathcal{C}_{11}^{(-)} \right] e + \mathcal{O}(e^2) \right\}. \end{aligned} \quad (49)$$

Putting all this together, the square $|\delta\tilde{\mathbf{r}}|^2$ of the normalized perturbed displacement can be expressed as

$$|\delta\tilde{\mathbf{r}}|^2 = \left[\sin \xi \mathcal{S}_{11}^{(+)} + \cos \xi \mathcal{C}_{11}^{(-)} \right]^2 + 4 \left[2 \left(\sin(\omega_a t + \alpha) - \sin \alpha \right) + \sin \xi \mathcal{C}_{11}^{(-)} - \cos \xi \mathcal{S}_{11}^{(+)} \right]^2 + \mathcal{O}(e). \quad (50)$$

Integrating this expression from $t = 0$ until $t = t_{\text{obs}}$ returns terms linear in t_{obs} along with a transient contribution that vanishes in the limit $t_{\text{obs}} \rightarrow \infty$. We shall mainly focus on the former in the following discussion since it solely survives for large ξ_{obs} , which is the experimental setup considered here. However, we will also show the full result for the sake of comparison with the data.

4.3. The case $e = 0$

For a circular orbit, the value of the initial mean anomaly \mathcal{M}_0 and the phase α of the axion field are irrelevant to the signal-to-noise ratio. Therefore, we can choose $\mathcal{M}_0 = \alpha = 0$ without any restriction. With this simplification, a straightforward calculation shows that

$$\frac{1}{\xi_{\text{obs}}} \int_0^{\xi_{\text{obs}}} d\xi |\delta\tilde{\mathbf{r}}|^2(\xi) = \mathcal{R}_\infty \left(\frac{\Omega}{\omega_a} \right) + \text{transient}. \quad (51)$$

The transient contribution is of the form

$$\sum_i c_i \frac{\sin(\varpi_i \xi_{\text{obs}})}{\varpi_i \xi_{\text{obs}}}, \quad (52)$$

where the various amplitudes c_i and frequencies ϖ_i (loosely labelled with an index i) are functions of the frequencies ω_a and Ω . Its explicit expression - which is subdominant in the long-time asymptotic limits - is too long to be given here. The response function $\mathcal{R}_\infty(x)$ - which dominates in the long-time asymptotic limit - takes the form

$$\mathcal{R}_\infty(x) = 8x^2 \frac{\left(\frac{3}{2} + x^2\right)}{(1 - x^2)^2}. \quad (53)$$

It diverges at the fundamental resonance $x = 1$, and its asymptotic behaviour as the argument tends towards

zero or infinity is

$$\mathcal{R}_\infty(x) = \begin{cases} 12x^2 + \mathcal{O}(x^4) & (x \rightarrow 0) \\ 8 + 28x^{-2} + \mathcal{O}(x^{-4}) & (x \rightarrow \infty) \end{cases}. \quad (54)$$

Unsurprisingly, $\mathcal{R}_\infty(x)$ is analogous to the response function (or transfer function) of a standard driven harmonic oscillator of frequency Ω , in which the axion oscillations $\propto \sin(\Omega t/x + \alpha)$ play the role of the external driving force (this can also be seen upon writing the orbit equation for $u(\vartheta)$, where $u \equiv 1/r$). In the limit $x \rightarrow 0$ (slow driving), this force can be treated as constant and, therefore, $\mathcal{R}_\infty(x) \rightarrow \text{const.}$ since the displacement is independent of frequency. In the limit $x \rightarrow \infty$ (fast driving), the constant (i.e. frequency-independent) terms in Eq.(50) cancel out so that the response function is proportional to $x^2 \sim (\omega_a)^{-2}$. All this remains true when $e > 0$ (see Sec. §4.4).

Substituting the response function into Eq.(40), the long-time signal-to-noise reads

$$\left(\frac{S}{N}\right)^2 = \left(\frac{\epsilon \Omega a}{\omega_a}\right)^2 \frac{f_{\text{obs}} t_{\text{obs}}}{\sigma_\Delta^2 c^2 \Delta} \mathcal{R}_\infty\left(\frac{\Omega}{\omega_a}\right). \quad (55)$$

Using Eq.(43), the SNR expressed as a function of the semi-major axis a scales like

$$\left(\frac{S}{N}\right) \propto \begin{cases} a^{5/2} & (a \ll a_0) \\ a & (a \gg a_0) \end{cases} \quad (56)$$

The $a^{5/2}$ behaviour in the regime $a \ll a_0$ reflects the scaling $\mathcal{R}_\infty(x) \rightarrow \text{const.}$ of the response function for large orbital frequencies $x \gg 1$.

Our prediction with the response function Eq.(53) is shown in Fig.2 as the solid (red) curve. The overlaid dashed (magenta) curve represents the full result (i.e. including the transient contribution). For comparison, the blue data points indicate the simulated SNR for a circular orbit. Note that we have artificially increased ϵ_0 by a factor of 10^5 in order to reduce the numerical noise.

4.4. The case $0 < e < 1$

When the eccentricity is different from zero, the perturbation to the Keplerian frequency Eq. (36) provides the greatest contribution to the signal across the lowest order resonances in the limit $t_{\text{obs}} \gg \Omega^{-1}$ since the amplitude of this effect grows like $(\Omega t)^2$. The variation of the Keplerian frequency (unlike a simple one-dimensional harmonic oscillator for which the fundamental frequency is fixed) leads to a infinite series of resonances located at $k\Omega = \omega_\alpha$, with $k \in \mathbb{N}$.

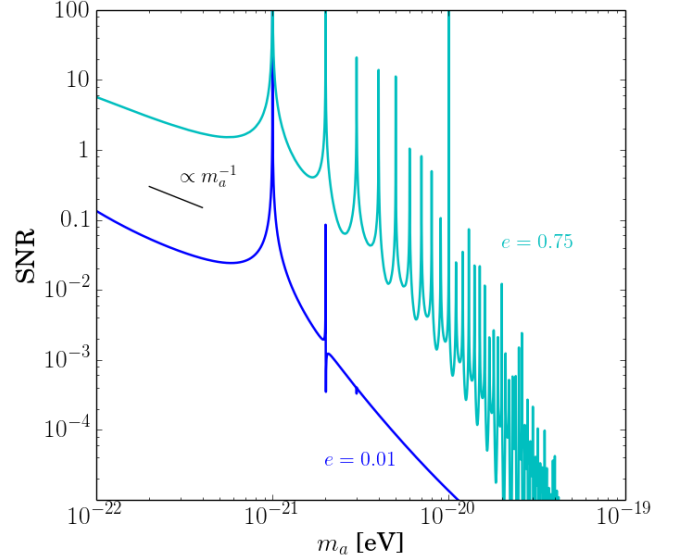


Figure 3. Signal-to-noise ratio as a function of the axion mass m_a when the orbital parameter are fixed to their fiducial value (see Sec. §2). Results are shown for a near circular ($e = 0.01$) and highly eccentric ($e = 0.75$) orbit. For small axion masses $m_a \ll \Omega_0$, the SNR scales like m_a^{-1} as indicated on the figure.

4.4.1. Perturbation to the orbital frequency

The term proportional to \mathcal{A}_n in Eq.(36) dominates the perturbation to the orbital frequency. Since a change in the latter affects θ_c solely, its contribution to the SNR of the Roemer time delay is given by

$$\begin{aligned} & \frac{1}{\xi_{\text{obs}}} \int_{\xi_0}^{\xi_{\text{obs}} + \xi_0} d\xi (1 - e \cos \xi) \left[\left(\frac{\partial \tilde{r}}{\partial \theta_c} \right)^2 + \tilde{r}^2 \left(\frac{\partial \vartheta}{\partial \theta_c} \right)^2 \right] \times 36(\Omega t)^2 \left\{ \sum_{n=1}^{\infty} \frac{J_n(ne)}{n} \mathcal{A}_n \left(\frac{\Omega}{\omega_a}, \alpha, \mathcal{M}_0 \right) \right\}^2 \\ &= 36 \times \left\{ \frac{1}{\xi_{\text{obs}}} \int_{\xi_0}^{\xi_{\text{obs}} + \xi_0} d\xi (1 + e \cos \xi) (\mathcal{M}(\xi) - \mathcal{M}_0)^2 \right\} \times \left\{ \sum_{n=1}^{\infty} \frac{J_n(ne)}{n} \mathcal{A}_n \left(\frac{\Omega}{\omega_a}, \alpha, \mathcal{M}_0 \right) \right\}^2. \end{aligned} \quad (57)$$

For large values of $\xi_{\text{obs}} \gg \xi_0$, the integral over the eccentric anomaly (as emphasized by the curly brackets)

asymptotes to ξ_{obs}^2 in the long-time limit, with transient

residuals proportional to ξ_{obs} (in the best case) that can safely be neglected. Therefore, the frequency change yields a contribution

$$\mathcal{R}_{\infty} \supset 12 \xi_{\text{obs}}^2 \left[\sum_{n=1}^{\infty} \frac{J_n(ne)}{n} \mathcal{A}_n \left(\frac{\Omega}{\omega_a}, \alpha, \mathcal{M}_0 \right) \right]^2 \quad (58)$$

to the response function. As we will see shortly, it depends sensitively on the axion phase α and the initial condition \mathcal{M}_0 . Since, at fixed t_{obs} , the total observed lapse of eccentric anomaly is $\xi_{\text{obs}} \propto \Omega$, the correspond-

ing signal-to-noise decays like $\propto a^{-1/2}$ for $a > a_0$ and eventually drops below the signal-to-noise $\propto a$ arising from the other perturbations.

4.4.2. Instantaneous perturbations

To calculate the combined effect of these instantaneous perturbations, we must, here again, take into account all the resonances because they lead to the cancellation of the zeroth order term $\propto \Omega^0$, such that the behaviour $S/N \propto a$ is recovered in the regime $\Omega \rightarrow 0$. We demonstrate this point in Appendix §A. Alternatively, notice that

$$\begin{aligned} \delta q_{\alpha}(t) &= \frac{\partial q_{\alpha}}{\partial \theta_{\alpha}}(t) \Delta \theta_{\alpha}(t) + \frac{\partial q_{\alpha}}{\partial J_{\alpha}}(t) \Delta J_{\alpha}(t) \\ &= \int_0^t dt' [q_{\alpha}(t), \mathcal{H}_1(t')]_{\theta_{\alpha}, J_{\alpha}} \\ &= 4\pi G \rho_{\text{DM}} \mu \int_0^t dt' \cos(\omega_a t' + \alpha) r(t') [q_{\alpha}(t), r(t')]_{\theta_{\alpha}, J_{\alpha}} \\ &= 4\pi G \rho_{\text{DM}} \mu \int_{\xi_0}^{\xi_{\text{obs}} + \xi_0} d\xi' (1 - e \cos \xi') \cos(\omega_a t'(\xi') + \alpha) r(\xi') [q_{\alpha}(\xi), r(\xi')]_{\theta_{\alpha}, J_{\alpha}}. \end{aligned} \quad (59)$$

where $q_{\alpha} = \{r, \vartheta\}$ are the polar coordinates. We have ignored the frequency change arising from \mathcal{H}_0 (since we treat it separately). In the limit $\Omega \rightarrow 0$, the variable t evolves independently of the eccentric anomaly, which remains constant and equal to $\xi \equiv \xi_0$ during the entire observational period. As a result, the Poisson brackets converges towards $[q_{\alpha}(\xi_0), r(\xi_0)]$, which must vanish by definition. Therefore, there is no contribution to the signal-to-noise proportional to $\epsilon \cdot \Omega \cdot a \sim a^{5/2}$ in the limit $\Omega \rightarrow 0$.

To derive the leading non-vanishing contribution, we expand the functions \mathcal{S} and \mathcal{C} that appear in Eqs.(30) – (33) in the small ratio Ω/ω_a as in Eq.(A2). Namely, we must retain the argument $n\Omega t$ of the trigonometric functions because t can be arbitrary large and, thus, Ωt is not necessarily small.

Obtaining the exact functional dependence on e , α and \mathcal{M}_0 is challenging owing to the presence of a multiplicative factor of $(1 - e \cos \xi)^{-1}$. A rough approximation can be derived upon treating t and ξ as independent variables (an approximation justified by the fact that the frequencies Ω and ω_a are vastly different) and setting $\xi = \xi_0$ (which has the advantage of removing factors of $(1 - e \cos \xi)^{-1}$ in the integrand). Successively averaging over t (with $0 \leq t < 2\pi/\omega_a$) and ξ (with $0 \leq \xi < 2\pi/\Omega$),

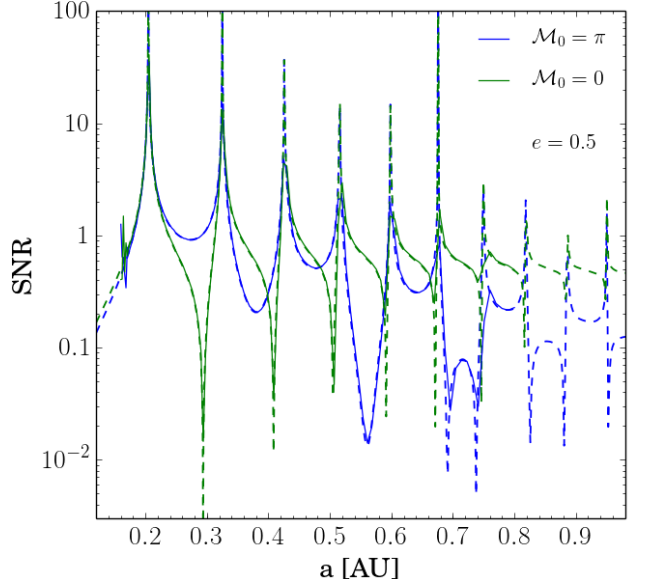


Figure 4. Dependence of the SNR on the initial conditions. The solid and dashed curves show the simulation and theoretical prediction for $\mathcal{M}_0 = 0$ (blue) and $\mathcal{M}_0 = \pi$ (green). Results are shown for an unperturbed Keplerian orbit with $e = 0.5$. An axion phase $\alpha = 0$ is assumed throughout.

we eventually arrive at

$$\mathcal{R}_\infty \supset 2 \left(\frac{\Omega}{\omega_a} \right)^2 (1 + 33e^2) (2 + \cos 2\alpha) . \quad (60)$$

Although the dependence on α is certainly incorrect (in the limit $e \rightarrow 0$, any dependence on α should vanish as outlined in Sec. §4.3), this shows that the amplitude of this effect mildly increases with the eccentricity.

4.4.3. Response function for $0 < e < 1$

In analogy with the circular case, the signal-to-noise for $0 < e < 1$ can be recast into the form

$$\left(\frac{S}{N} \right)^2 = \left(\frac{\epsilon \Omega a}{\omega_a} \right)^2 \frac{f_{\text{obs}} t_{\text{obs}}}{\sigma_\Delta^2 c^2 \Delta} \mathcal{R}_\infty \left(\frac{\Omega}{\omega_a}, e, \alpha, \mathcal{M}_0; \Omega t_{\text{obs}} \right) \quad (61)$$

in which the response function \mathcal{R}_∞ is the sum of Eq.(58) and Eq.(60). The SNR behaves like

$$\left(\frac{S}{N} \right) \propto \begin{cases} a^{5/2} & (a \ll a_0) \\ a^{-1/2} & (a \sim a_0) \\ a & (a \gg a_0) \end{cases} , \quad (62)$$

where $a \sim a_0$ signifies "in the resonant region". As emphasized earlier, this behaviour is consistent with the response of an harmonic oscillator to an external, oscillatory perturbation.

When the SNR is shown as a function of axion mass m_a for a fixed orbital configuration (as would arise from the analysis of a given pulsar timing residuals series), Eq.(62) gives the behaviour $\propto m_a^{-1}$ for $m_a \ll \Omega_0$, and $\propto m_a^{-2}$ for $m_a \gg \Omega_0$. This behaviour can be seen in Fig.3, where the sensitivity curve is shown for two different eccentricities.

4.5. Validation with numerical simulations

In all subsequent illustrations, the theory curve represents the long-time asymptotic result characterized by the response function \mathcal{R}_∞ (that is, we neglect the transient contribution).

Fig.4 demonstrates the impact of the initial mean anomaly on the SNR. When $\mathcal{M}_0 = 0$ or π , the response function simplifies to

$$\mathcal{R}_\infty(x, e, \alpha, \mathcal{M}_0; \xi_{\text{obs}}) = 48 \xi_{\text{obs}}^2 \left[\sum_{n=1}^{\infty} \sigma(n) \frac{x J_n(ne)}{(1 - n^2 x^2)} \right]^2$$

with $\begin{cases} \sigma(n) = 1 & (\mathcal{M}_0 = 0) \\ \sigma(n) = (-1)^n & (\mathcal{M}_0 = \pi) \end{cases}$ (63)

The resonant patterns vary significantly (the difference can exceed an order of magnitude at a given eccentricity)

across the range of values spanned by a . Near the resonances, the discrepancy between the numerical data and the theoretical predictions is due to transients, which are negligible away from resonances provided that t_{obs} is larger than a few orbital times.

Fig.5 compares the prediction Eq.(61) (dashed curves) to the numerical result (solid curves) for different values of the eccentricity. The model parameters are $\mathcal{M}_0 = \pi$ and $\alpha = 0$. The agreement between theory and simulations is excellent for all the configurations considered here.

For the range of semi-major axis values shown here, the contribution Eq.(58) dominates the SNR shown in Figures 4 and 5. Notwithstanding, the contribution Eq.(60) turns out to be significant for the nearly circular orbit with $e = 0.01$ above $a \gtrsim 0.5$ AU.

4.6. Gravitational wave emission

We have not considered the loss of energy through the emission of gravitational radiation. Ignoring the dependence on eccentricity, the power radiated in gravitational waves during one orbital period is (Peters 1964)

$$P_{\text{GW}} = \frac{32}{5c^5} \mu^2 G^{7/3} M^{4/3} \Omega^{10/3} . \quad (64)$$

By comparison, the power injected by the axion coherent oscillations during one orbital period is

$$P_a \sim \epsilon \mu \Omega^2 a^2 \cdot \Omega = \epsilon \mu G^{2/3} M^{2/3} \Omega^{5/3} . \quad (65)$$

Therefore, ignoring factors of order unity and assuming $\Omega \sim \omega_a$, we find

$$\frac{P_{\text{gw}}}{P_a} \sim \frac{\mu}{\epsilon} G^{5/3} M^{2/3} \Omega^{5/3} \sim (10^{18} \epsilon)^{-1} \quad (66)$$

upon inserting our fiducial orbital parameters. This ratio is very small for the default value of ϵ adopted here (see Eq.(6), but it would be of order unity for a dark matter density comparable to that of the solar neighborhood. In this case, we expect that the damping produced by gravitational wave emission smoothes the response function around the resonances (in analogy with a simple one-dimensional damped, driven harmonic oscillator).

Since P_{GW}/Ω is very small compared to the binding energy of the system (except for the very last stages of the merger), the orbits shrink adiabatically owing to the emission of gravitational radiation. Using the classical formula Eq.(64), the time spent in a semi-major axis interval of width $\Delta a \sim \sqrt{\epsilon}$ is

$$t_{\text{res}} \sim \frac{5}{154} \frac{c^5}{G^3 \mu M^2} a^3 \Delta a . \quad (67)$$

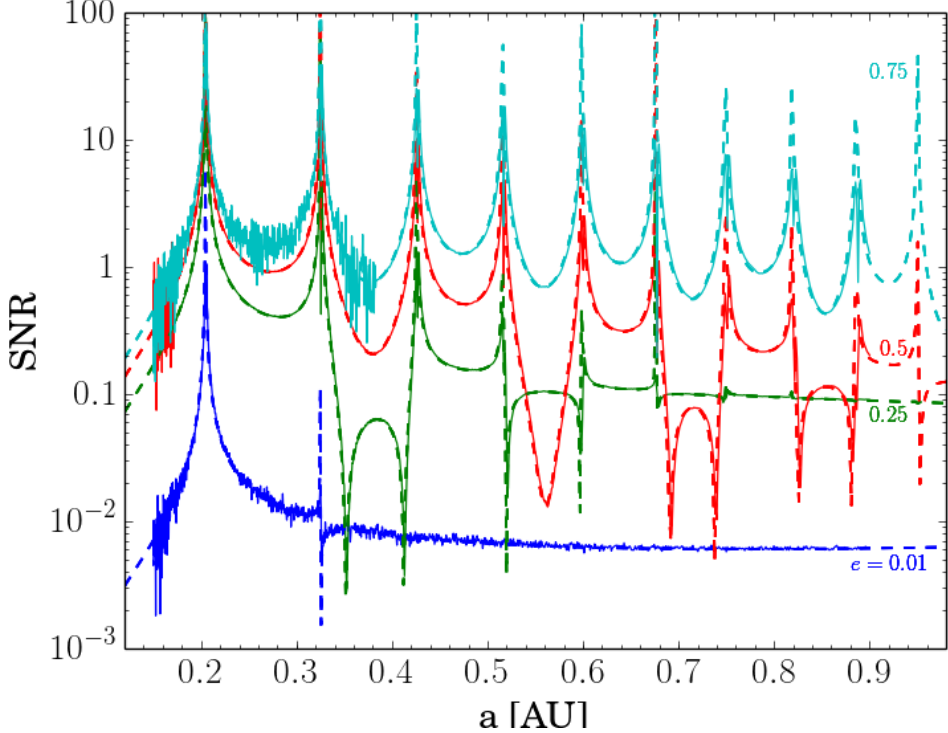


Figure 5. Signal-to-noise for various eccentricities $0 < e < 1$. The solid and dashed curves show the simulations and theoretical predictions for $e = 0.01$ (blue), 0.25 (green), 0.5 (red) and 0.75 (cyan), respectively. The initial mean eccentricity is $\mathcal{M}_0 = \pi$. The data shown here is also displayed in Fig.4 of [Rozner et al. \(2019\)](#).

Consider now the fundamental resonance centered at $\Omega = \omega_a$. Using the techniques presented in [Rozner et al. \(2019\)](#), the width of the corresponding resonant region (that is, the libration region which cannot be resolved with our perturbative approach) is

$$\Delta a = \sqrt{\frac{32\epsilon J_1(e)}{3}} a_0. \quad (68)$$

Therefore, taking $e = 0.5$ for illustration, the time spent in the fundamental resonance is

$$t_{\text{res}} \approx 0.05 \frac{c^5 a_0^4}{G^3 \mu M^2} \sqrt{\epsilon_0}. \quad (69)$$

For our fiducial parameter values, we obtain $t_{\text{res}} \approx 6.1 \times 10^7$ yr. This shows that, for the orbital parameters adopted here, the system would stay at resonance for a duration much longer than any realistic observational time. In practice however, the probability that a binary system will be found at resonance is very small owing to the smallness of $\sqrt{\epsilon}$, and the calculation presented in this paper will apply for most of the parameter space.

5. CONCLUSIONS

We investigated the instantaneous variations produced by the coherent oscillations of ultra-light axion dark matter on a Keplerian binary. After solving the equations of motion at first order in the (small) perturbations, we focused on the response of the binary separation to this oscillatory driving force, the amplitude of which can be constrained with pulsar timing owing to its impact on the Roemer time delay.

We computed the signal-to-noise ratio for a measurement of instantaneous variations in the Roemer time delay, providing physical intuition whenever possible. In particular, we emphasized its similarity with the response of an harmonic oscillator to an external oscillatory driving (unsurprising, given the duality between the Kepler problem and the 2-dimensional harmonic oscillator, see [Arnol'd 1990](#)). We outlined the dependence of such a measurement on the orbital parameters as well as the initial axion and orbital phases. We compared our theoretical predictions to accurate numerical simulations and found excellent agreement for a wide range of eccentricities $0 \leq e < 1$. Although we did not consistently include the back reaction of the binary system, which can emit energy in the form of gravitational waves etc. (see e.g. [Annunzi et al. 2018](#), for a recent discussion), these effects should be negligible unless the binary is

about to merge. Furthermore, we ignored the orientation of the orbital plane relative to the line-of-sight to the observer for simplicity, but this can be easily taken into account.

Our exact expressions furnish a useful benchmark for numerical codes and analysis procedures and, hopefully, will motivate the search for such imprints in real data. While we concentrated on dark matter in the form of a Bose-Einstein condensate of ultra-light axions (for which the signal induced by oscillations in the gravitational po-

tential is arguably small), our application of the angle-action formalism can, of course, be extended to other dark matter scenarios and/or different couplings (see e.g. Blas et al. 2017; Nojiri et al. 2019)

ACKNOWLEDGMENTS

V.D. and Y.B.G. acknowledge support by the Israel Science Foundation (grant no. 1395/16).

APPENDIX

A. PERTURBATIONS IN THE LIMIT $\Omega \rightarrow 0$

We consider the regime $\Omega \ll \omega_a$ and expand the functions $\mathcal{S}_{n1}^{(+)}$ and $\mathcal{C}_{n1}^{(-)}$ that appear in Eqs.(30) – (33) accordingly to obtain

$$\begin{aligned}\mathcal{S}_{n1}^{(+)} &\approx 2 \left(\sin(\omega_a t + \alpha) \cos(n\mathcal{M}) - \sin \alpha \cos(n\mathcal{M}_0) \right) - 2n \left(\frac{\Omega}{\omega_a} \right) \left(\cos(\omega_a t + \alpha) \sin(n\mathcal{M}) - \cos \alpha \sin(n\mathcal{M}_0) \right) \quad (A1) \\ \mathcal{C}_{n1}^{(-)} &\approx -2 \left(\sin(\omega_a t + \alpha) \sin(n\mathcal{M}) - \sin \alpha \sin(n\mathcal{M}_0) \right) - 2n \left(\frac{\Omega}{\omega_a} \right) \left(\cos(\omega_a t + \alpha) \cos(n\mathcal{M}) - \cos \alpha \cos(n\mathcal{M}_0) \right).\end{aligned}$$

In the limit $\Omega \rightarrow 0$, only the first term subsists in the right-hand side of Eq.(A2). Furthermore, $\mathcal{M} \approx \mathcal{M}_0$ since the mean anomaly does not change appreciably during the observational period. Therefore, we find

$$\begin{aligned}\mathcal{S}_{n1}^{(+)} &\stackrel{\Omega \rightarrow 0}{=} 2 \left(\sin(\omega_a t + \alpha) - \sin \alpha \right) \cos(n\mathcal{M}_0) \quad (A2) \\ \mathcal{C}_{n1}^{(-)} &\stackrel{\Omega \rightarrow 0}{=} -2 \left(\sin(\omega_a t + \alpha) - \sin \alpha \right) \sin(n\mathcal{M}_0).\end{aligned}$$

Substituting these expressions into Eqs.(30) – (33) and taking advantage of the relations

$$\begin{aligned}\sum_{n=1}^{\infty} J_n(ne) \cos(n\mathcal{M}) &= \frac{e \cos \xi}{2(1 - e \cos \xi)} \quad (A3) \\ \sum_{n=1}^{\infty} \frac{J_n(ne)}{n} \sin(n\mathcal{M}) &= \frac{e}{2} \sin \xi,\end{aligned}$$

the series expansions of $\Delta\theta_b$, $\Delta\theta_c$ and ΔJ_c become

$$\begin{aligned}\Delta\theta_b &\approx 2\epsilon \left(\frac{\Omega}{\omega_a} \right) \frac{\sqrt{1 - e^2}}{e} \left(\cos \xi_0 - e \right) \left(\sin(\omega_a t + \alpha) - \sin \alpha \right) + \dots \quad (A4) \\ \Delta\theta_c &\approx 2\epsilon \left(\frac{\Omega}{\omega_a} \right) \left[3 - \left(\frac{1}{e} + 3e \right) \cos \xi_0 + e^2 \cos(2\xi_0) \right] \left(\sin(\omega_a t + \alpha) - \sin \alpha \right) + \dots \\ \Delta J_c &\approx -2\epsilon J_c \left(\frac{\Omega}{\omega_a} \right) e \sin \xi_0 \left(\sin(\omega_a t + \alpha) - \sin \alpha \right) + \dots\end{aligned}$$

in the limit $\Omega \rightarrow 0$. On setting $\xi = \xi_0$ in Eqs. (25) and (28) (but allowing t to grow freely) and taking into account the leading contribution in Eq.(A4) solely, we can check that

$$\begin{aligned}\delta r &= \frac{\partial r}{\partial \theta_c}(\xi_0) \Delta\theta_c + \frac{\partial r}{\partial J_c}(\xi_0) \Delta J_c \quad (A5) \\ &= \epsilon a \left(\frac{\Omega}{\omega_a} \right) \left\{ \left(\frac{e \sin \xi_0}{1 - e \cos \xi_0} \right) 2 \left[3 - \left(\frac{1}{3} + 3e \right) \cos \xi_0 + e^2 \cos(2\xi_0) \right] \right\}\end{aligned}$$

$$\begin{aligned}
& - \frac{(-3e + \cos \xi_0 + 3e^2 \cos \xi_0 - e^3 \cos(2\xi_0))}{e(e \cos \xi_0 - 1)} 2e \sin \xi_0 \Big\} \Big(\sin(\omega_a t + \alpha) - \sin \alpha \Big) \\
& \equiv 0 ,
\end{aligned}$$

as the curly brackets identically vanishes regardless the value of ξ_0 . Similar manipulations lead to $\delta\vartheta \equiv 0$ under the same assumptions. This implies that the response function must scale like $\mathcal{R}_\infty \propto (\Omega/\omega_a)^2$ for small Ω/ω_a .

REFERENCES

Annunli, L., Bernard, L., Blas, D., & Cardoso, V. 2018, Phys. Rev. D, 98, 084001

Armengaud, E., Palanque-Delabrouille, N., Yche, C., Marsh, D. J. E., & Baur, J. 2017, Mon. Not. Roy. Astron. Soc., 471, 4606

Arnol'd, V. I. 1990, Huygens and Barrow, Newton and Hooke. Pioneers in mathematical analysis and catastrophe theory from evolvents to quasicrystals.

Bar, N., Blum, K., Lacroix, T., & Panci, P. 2019, JCAP, 2019, 045

Binney, J., & Tremaine, S. 1987, Galactic dynamics

Blas, D., Lpez Nacir, D., & Sibiryakov, S. 2019, arXiv:1910.08544

Blas, D., Nacir, D. L., & Sibiryakov, S. 2017, Phys. Rev. Lett., 118, 261102

Bokovi, M., Duque, F., Ferreira, M. C., Miguel, F. S., & Cardoso, V. 2018, Phys. Rev., D98, 024037

Broadhurst, T., de Martino, I., Luu, H. N., Smoot, G. F., & Tye, S. H. H. 2019, arXiv:1902.10488

Chavanis, P.-H. 2011, Phys. Rev., D84, 043531

Davies, E. Y., & Mocz, P. 2020, Mon. Not. R. Astron. Soc., 492, 5721

De Martino, I., Broadhurst, T., Tye, S.-H. H., et al. 2017, Physical Review Letters, 119, 221103

Desjacques, V., & Nusser, A. 2019, Mon. Not. R. Astron. Soc., 488, 4497

Edwards, R. T., Hobbs, G. B., & Manchester, R. N. 2006, Mon. Not. R. Astron. Soc., 372, 1549

Gonzlez-Morales, A. X., Marsh, D. J. E., Pearrubia, J., & Urea-Lpez, L. A. 2017, Mon. Not. Roy. Astron. Soc., 472, 1346

Hellings, R. w., & Downs, G. s. 1983, Astrophys. J., 265, L39

Hlozek, R., Marsh, D. J. E., & Grin, D. 2018, Mon. Not. Roy. Astron. Soc., 476, 3063

Hui, L., McWilliams, S. T., & Yang, I.-S. 2013, Phys. Rev., D87, 084009

Hui, L., Ostriker, J. P., Tremaine, S., & Witten, E. 2017, Phys. Rev. D, 95, 043541

Iršič, V., Viel, M., Haehnelt, M. G., Bolton, J. S., & Becker, G. D. 2017, Phys. Rev. Lett., 119, 031302

Khelnitsky, A., & Rubakov, V. 2014, JCAP, 1402, 019

Kobayashi, T., Murgia, R., De Simone, A., Iri, V., & Viel, M. 2017, Phys. Rev., D96, 123514

Marsh, D. J. E. 2016, Phys. Rep., 643, 1

Marsh, D. J. E., & Pop, A.-R. 2015, Mon. Not. Roy. Astron. Soc., 451, 2479

Mashhoon, B. 1978, Astrophys. J., 223, 285

—. 1985, Mon. Not. R. Astron. Soc., 217, 265

Mashhoon, B., Carr, B. J., & Hu, B. L. 1981, Astrophys. J., 246, 569

Niemeyer, J. C. 2019, arXiv:1912.07064

Nojiri, S., Odintsov, S. D., Oikonomou, V. K., & Popov, A. A. 2019, Phys. Rev., D100, 084009

Peters, P. C. 1964, Phys. Rev., 136, B1224

Porayko, N. K., & Postnov, K. A. 2014, Phys. Rev., D90, 062008

Porayko, N. K., Zhu, X., Levin, Y., et al. 2018, Phys. Rev. D, 98, 102002

Rein, H., & Liu, S.-F. 2012, Astron. Astrophys., 537, A128

Rein, H., & Spiegel, D. S. 2015, Mon. Not. R. Astron. Soc., 446, 1424

Rozner, M., Grishin, E., Ginat, Y. B., Igoshev, A. P., & Desjacques, V. 2019, arXiv:1904.01958

Rudenko, V. N. 1975, Soviet Ast., 19, 270

Safarzadeh, M., & Spergel, D. N. 2019, arXiv:1906.11848

Turner, M. S. 1979, Astrophys. J., 233, 685

Wasserman, A., et al. 2019, arXiv:1905.10373